AAEC/E254

AUSTRALIAN ATOMIC ENERGY COMMISSION

RESEARCH ESTABLISHMENT
LUCAS HEIGHTS

TIME DEPENDENT ^{237}Np, ^{235}U AND ^{239}Pu FISSION RATES IN A THORIUM ASSEMBLY DURING THE INTERVAL 0 TO 200 ns USING A PULSED ^{9}Be(d,n) SOURCE

PART 1 - EXPERIMENT

by

S.P. MOO*
M.T. RAINBOW
A.I.M. RITCHIE

* University of Tasmania, Hobart

March 1973

ISBN 0 642 99540 0

AUSTRALIAN ATOMIC ENERGY COMMISSION

RESEARCH ESTABLISHMENT

LUCAS HEIGHTS

TIME DEPENDENT ^{237}Np, ^{235}U AND ^{239}Pu FISSION RATES IN A THORIUM ASSEMBLY DURING THE INTERVAL 0 TO 200 ns USING A PULSED $^{9}Be(d,n)$ SOURCE

PART I – EXPERIMENT

by

S. P. MOO *

M. T. RAINBOW **

A. I. M. RITCHIE **

ABSTRACT

This paper describes a series of integral pulsed neutron experiments performed in a 0.4 x 0.4 x 0.4 m^3 metallic thorium assembly in such a way as to allow direct comparison of space independent reaction rates with calculated reaction rates derived from a code which uses the asymptotic reactor theory approximation to describe leakage. The technique relies on the Fourier decomposition of measured space-time dependent reaction rates and the extraction from these of the reaction rate corresponding to the fundamental three-dimensional Fourier spatial mode. The reaction rates measured were the fission rates of ^{235}U, ^{239}Pu and ^{237}Np following a short (~ 10 ns) burst of neutrons with a mean energy of ~ 2.7 MeV.

* University of Tasmania, Hobart

** A.A.E.C. Research Establishment, Lucas Heights, N.S.W.

National Library of Australia card number and ISBN 0 642 99540 0

The following descriptors have been selected from the INIS Thesaurus to describe the subject content of this report for information retrieval purposes. For further details please refer to IAEA--INIS--12 (INIS: Manual for Indexing) and IAEA–INIS–13 (INIS: Thesaurus) published in Vienna by the International Atomic Energy Agency.

BOUNDARY CONDITIONS; DECAY; ERRORS; FAST NEUTRONS; FISSION; FOURIER ANALYSIS; MEV RANGE 01–10; NEPTUNIUM 237; NEUTRON BEAMS; NEUTRON DETECTION; NEUTRON LEAKAGE; NEUTRON SOURCES; NUCLEAR REACTION KINETICS; PLUTONIUM 239; PULSED NEUTRON TECHNIQUES; PULSES; SPATIAL DISTRIBUTION; SUBCRITICAL ASSEMBLIES; THREE-DIMENSIONAL CALCULATIONS; THORIUM; TIME DEPENDENCE; TIME-OF-FLIGHT METHOD; URANIUM 235

CONTENTS

1. INTRODUCTION

The pulsed neutron technique has been most widely used in the investigation of thermal neutron assemblies (see Beckurts (1965) for review article), but during the last decade it has been extended to the study of fast neutron assemblies. In most of the thermal systems studied there was an asymptotic mode of decay and hence it was possible to measure unambiguously a decay constant which was related in a well defined way to the thermal diffusion parameters. In fast non-multiplying assemblies, no such asymptotic mode of decay exists, principally because there is no upscattering in such systems. The neutrons are continuously slowed down to lower energies and the neutron energy spectrum changes continuously with time. Hence the simple analysis used in the study of thermal systems by the pulsed technique is not possible in general. However, the fact that the neutron energy spectrum changes continuously with time can be used to advantage since any given reaction rate samples neutrons of different energies and hence neutrons interacting with the transport medium in different ways at different times after the pulse.

Several integral pulsed experiments with fast non-multiplying assemblies have been reported in the literature. Beghian et al.(1963 a and b, 1965, 1967) have measured leakage rates of essentially monoenergetic neutrons from iron, lead, bismuth and natural uranium assemblies. Similar measurements have been performed by Deconninck et al. (1965) with iron, copper and graphite assemblies and by Miessner and Arai (1966, also Arai et al. 1966) with lead and natural uranium assemblies. Napolitano et al. (1969, 1970) have performed pulse propogation experiments with an iron assembly. Time dependent fission rates of various elements have been measured in depleted uranium assemblies by Kato et al. (1965) and more recently by Gozani (1969). Kato et al. measured time dependent fission rates of ^{233}U, ^{235}U, ^{237}Np, ^{239}Pu and ^{240}Pu and also measured energy spectra by a pulsed time-of-flight technique. Gozani measured the time dependent fission rates of ^{235}U and ^{237}Np.

This paper describes a series of integral pulsed neutron experiments performed in a 0.4 x 0.4 x 0.4 m^3 metallic thorium assembly in such a way as to allow direct comparison of space independent reaction rates with calculated reaction rates derived from a code which uses the asymptotic reactor theory approximation to describe leakage. The technique, which was developed previously (Rainbow and Ritchie 1971) in a study of the slowing down processes in a thermal system, relies on the Fourier decomposition of measured space-time dependent reaction rates and the extraction from these of the reaction rate corresponding to the fundamental three-dimensional Fourier spatial mode. Three sets of measurements were performed which consisted of measuring the fission rates of ^{237}Np, ^{235}U and ^{239}Pu respectively, following a short ($\sim$ 10 ns) burst of neutrons with a mean energy of $\sim$ 2.7 MeV.

2. APPARATUS AND EXPERIMENTAL METHOD

2.1 Thorium Assembly

The thorium (Moo et al. 1972) was in the form of blocks, the majority of which were cubes of side 50.8 mm and each of which was coated with cellulose acetate lacquer to a thickness in the range 0.013 to 0.025 mm. These were stacked to form a rectangular parallelepiped (401.8 x 403.0 x 401.3 mm) with a 25.4 x 25.4 mm^2 hole through the centre to accommodate the

accelerator flight tube and three scan holes, each of cross section 13.1 x 13.1 mm running parallel to the flight tube (see Figure 1). A further scan hole running half the length of the stack was provided in the position shown for a monitor detector. The effective density of the thorium stack was 11.04 g cm^{-3} taking account of voidage due to the flight tube hole and the scan holes.

The thorium was supported on a three legged table with an 11 mm thick mild steel grate top at the centre of an experimental area, the ceiling of which was ~ 10.5 m above the floor. The floor, which was some 1.06 m below the centre of the stack, was covered in the immediate vicinity of the assembly with borated paraffin 150 mm thick. A 150 mm thick, 2.1 m high borated paraffin wall in the form of an approximate circle with internal diameter of ~ 3.8 m surrounded the assembly. Both the floor covering and the wall were intended to reduce the intensity and energy of the neutrons scattered back into the thorium stack. Further details of the stack and target arrangement are given elsewhere (Moo et al. 1972).

2.2 Neutron Detectors

The neutron detectors employed were Twentieth Century Electronics Limited, Type FC4B, cylindrical pulse fission chambers of cathode diameter 4.9 mm, anode diameter 1.6 mm and active length 25.4 mm. The fissile loadings were in the form of thin oxide films on the cathode of thickness 3 μg mm^{-2} for ^{237}Np and ^{239}Pu and 10 μg mm^{-2} for ^{235}U.

2.3 Pulsed Source

The basis of the pulsed neutron source was a 3 MeV Van de Graaff accelerator which was operated at 2.8 MeV in the 'nanosecond' pulsing mode both with and without klystron bunching. This allowed a range of beam pulse widths from about 4 ns to 15 ns at a repetition rate of 1 MHz. Neutrons were produced using the $^{9}Be(d,n)^{10}B$ reaction which, at a bombarding energy of 2.8 MeV has a rather complicated neutron spectrum (Inada et al. 1968) with an average energy of about 2.7 MeV and a marked forward peak in the angular distribution.

Throughout this investigation, the air cooled beryllium target was located at the centre of the stack. The target could also be removed from the path of the beam (see Figure 1) to allow the beam to impinge on a second target used to monitor the beam pulse profile. The monitoring was done at frequent intervals throughout each experiment by using an NE-102 plastic scintillator to detect the gamma ray burst emitted as the beam struck this second target.

2.4 Timing System

A block diagram of the timing system is shown in Figure 2 and is described in more detail elsewhere (Moo et al. 1972). However, several features require further comment.

The detector pulses were timed with respect to the leading edge of the beam pulse which was detected by a capacitive pick-off unit located in the flight tube 0.4 m from the target. The high and low level discriminator system on the output reduced both the timing jitter and the chances of spurious triggers from the high mass component in the unanalysed beam.

The preamplifiers used in conjunction with the detectors were fast current amplifiers built by Instrumentation and Control Division, Lucas Heights, to the specification of Rush (1964). Amplitude-risetime compensation (ARC) was used to provide timing signals from the detectors.

This was found to give much less timing uncertainty than crossover timing (Moo et al. 1972). For the first and second sets of measurements in which ^{237}Np and ^{235}U reaction rates were measured, the detector timing uncertainty was in the range ± 3.3 to ± 5.0 ns. For the third set, in which ^{239}Pu reaction rates were measured, the 'fraction' used in the ARC timing was decreased and the jitter also decreased to give a timing uncertainty in the range ± 2.2 to ± 3.4 ns.

A ^{237}Np pulse fission chamber was used to monitor source neutron production for normalisation purposes during the measurements of the ^{237}Np fission rate. A ^{235}U pulse fission chamber was used as a monitor during measurements with the broad range detectors. A gating system limited the scaling period of the monitor to ~ 300 ns in each cycle, this period starting some 15 ns before the rise of the reaction rate time distribution.

2.5 Method of Measurement

One of the main aims of this investigation was to extract the time dependent Fourier spatial modes, $R_{ijk}(t)$, for each reaction rate, and in particular, the fundamental mode $R_{111}(t)$. The theoretical basis of the technique has been described by Rainbow and Ritchie (1971).

The present investigation was confined to an interval of ~ 200 ns after the pulse. The decision to restrict the time interval was taken to avoid possible contribution from room return neutrons to measured broad range detector reaction rates. For example, the flight time of a 1 MeV neutron over a path of 2 m is 145 ns while the equivalent flight time of a 100 keV neutron is 457 ns. Thus, in the time interval up to 200 ns after the pulse, the number of neutrons scattered directly from the floor to a detector in the stack should be small and should be further reduced by the borated paraffin shielding. The time interval is, however, long compared to the 'decay time' for ^{237}Np (~ 15 ns) and is sufficiently long to place no significant limitations on measurements with this threshold detector.

Throughout the measurements the time to amplitude converter (TAC) was operated with a 1 μs time range and the analogue to digital converter (ADC) with 1024 channels. For the first and second sets of measurements the actual channel width was 1.245 ns and for the third set it was 1.18 ns, but in the analysis the data in consecutive pairs of channels were summed to give effective channel widths of 2.49 ns and 2.36 ns respectively. The timing of the start pulse with reference to the initial neutron pulse was such that the reaction rate was measured for some 150 ns before the start of the initial pulse. Although the main period of interest was restricted to some 200 ns after the pulse, the time range of 1 μs was used and measurement of the reaction rate at times before the pulse was done to allow an estimate to be made of the effect of background and overlap from earlier pulses (see Section 4.3).

The detectors were moved along aluminium tubes in the scan holes by a motorised screw device. At each spatial position the time distribution was measured for a preset monitor count. The positive logic output from the constant fraction timing discriminator was scaled to allow dead time correction in the TAC and ADC. The entire process of data taking and positioning of the detector along each scan hole was facilitated by a PDP-7 on-line computer.

Preliminary measurements along a transverse scan hole with a ^{237}Np detector showed that the transverse flux was symmetric, as was to be expected from the source conditions and that two cosines were sufficient to describe the transverse spatial distribution. For this reason, measurements were confined to three independent scan holes in the x direction and the analysis was confined to the extraction of the R_{i11}, R_{i13} and R_{i33} modes. It was assumed from symmetry that the R_{i13} and R_{i31} modes were identical.

For each detector, time distributions were measured at 13 positions (25 mm apart) in each of the three scan holes. Immediately before and at some stage during each spatial scan, the beam pulse profile was measured with the plastic scintillator. This allowed a check on the stability of the accelerator with regard to pulse shape. Spatial distributions in each of the scan holes were measured in rotation and then repeated at least once to average out the effect of longer term drift. The beam pulse shape throughout the measurements was approximately Gaussian. Table 1 lists the beam pulse widths, detector timing uncertainties and other details of the experiment.

TABLE 1

LIST OF EXPERIMENTAL PARAMETERS

	^{237}Np Experiment	^{235}U Experiment	^{239}Pu Experiment
Detector timing uncertainty* (ns)	± 3.3 to ± 5.0	± 3.3 to ± 5.0	± 2.2 to ± 3.4
Beam pulse width (ns, FWHM)	12.4	9.6	4.0
Actual channel width (ns)	1.245	1.245	1.18
Channel width (ns) used in analysis	2.49	2.49	2.36
Extrapolation length (mm)	42.6	29.0	30.5

x – dimension of assembly	401.8 mm
y – dimension of assembly	403.0 mm
z – dimension of assembly	401.3 mm
Effective density of assembly	11.04 g cm^{-3}

* We define the timing uncertainty to be the standard deviation of the timing uncertainty distribution. The values presented are estimated upper and lower bounds (see Moo et al. 1972).

3. DATA ANALYSIS AND RESULTS

3.1 Time Dependent Three-Dimensional Fourier Modes

Since the energy spectrum in the pulsed thorium assembly changes continuously with time, there is clearly a problem in choosing the appropriate extrapolation length both to describe the spatial distribution and to use it in the well known recipe to evaluate the buckling

term of the asymptotic reactor theory diffusion theory calculation. It should be stressed here that the objective in analysing the measured spatial distributions was to produce a space independent time dependent reaction rate that could be compared directly with the corresponding reaction rate calculated in a diffusion code which approximates leakage by a DB^2 term. It can easily be shown that to achieve this, the same extrapolated length must be employed in both the Fourier analysis of the experimental results and in calculating the buckling term used in the code. Furthermore, this extrapolated length must be time and energy independent (Ritchie and Moo 1972).

The problem then becomes one of choosing the most appropriate extrapolation length. There appears to be no clear criterion for choosing this although one such criterion would be that one mode (the fundamental) should decay more slowly than any other mode. Experimentally, this means that the fundamental mode would in time describe the spatial distribution. The extrapolation length used in the Fourier analysis of each reaction rate was one derived in the usual way from a transport mean free path which was averaged over a calculated time dependent energy spectrum and weighted according to the energy response of the detector. The thorium data were obtained from the ABBN set (Bondarenko 1964) and the detector fission cross sections were obtained from the Winfrith data file (Norton 1968). The actual values used for the extrapolation lengths were 42.6 mm, 29.0 mm and 30.5 mm for ^{237}Np, ^{235}U and ^{239}Pu respectively. The success of this choice can be judged from the fact that the decay rates of the higher spatial modes derived from the experiments were in all cases markedly faster than that of the fundamental mode (see Figure 4).

The method of Fourier mode decomposition was essentially the same as that described by Rainbow and Ritchie (1971). For each reaction rate, the time dependent spatial distribution along each scan hole was Fourier analysed using a weighted least square fitting routine, FORFIT. The Fourier amplitudes from the three independent scan holes allowed the time dependent three dimensional Fourier modes, $R_{ijk}(t)$, to be extracted.

Figure 3 presents the spatial distributions along scan hole A at several time channels for ^{237}Np and ^{235}U. It was found that the spatial distributions in the beam direction were adequately described by a sum of four cosines and two sines for both the threshold and broad range detectors. The three most significant three-dimensional Fourier modes are shown as a function of time in Figure 4a for ^{237}Np, in Figure 4b for ^{235}U and in Figure 4c for ^{239}Pu, while the amplitude and error of the fundamental mode are listed in Table 2 for the three fission rates. In all cases, the peak of the $R_{111}(t)$ mode has been arbitrarily assigned to channel No. 10.

3.2 Instantaneous Decay Constant

It is informative to examine the time dependence of the derivative of the reaction rate curves. This quantity is independent of any amplitude normalisation and is, therefore, useful in the comparison of measurements made at different positions or with different detectors. However, to obtain an estimate of the derivative with reasonable precision requires better statistical accuracy on the raw experimental data than is usually available. A useful approximation is to

assume that the decay curves are exponential over short time intervals and to evaluate 'instantaneous' decay constants, $\lambda(t)$, which are reasonable estimates of the time logarithmic derivative. This procedure has been used by other investigators (e.g. Gozani 1969) and is a convenient means of comparing data. However, care must be taken to ensure that the same procedures have been applied to all the data being intercompared.

A weighted least square fitting routine was used to calculate $\lambda(t)$. Each time distribution was fitted to a single exponential function over an interval of 11 channels (27.39 ns for the ^{237}Np and ^{235}U measurements and 25.96 ns for the ^{239}Pu measurements), the calculated $\lambda(t)$ being assigned to the middle channel. Successive $\lambda(t)$ were obtained by advancing the interval of fit.

Figure 5 shows the instantaneous decay constants for the time distributions of the ^{235}U detector at three positions (x = –100 mm, x = 0 mm and x = +100 mm) in scan hole A. The instantaneous decay constant of the lowest mode for the three fission rates are presented in Figure 6.

4. DISCUSSION OF ERRORS

4.1 Error Analysis in the Fourier Fitting Routine

The following errors were considered at each position of the time dependent spatial distribution along each scan hole:

(i) dead time correction in the channel counts,

(ii) statistical errors in the monitor counts,

(iii) statistical errors in the channel counts,

(iv) positioning error of each detector,

(v) timing uncertainty associated with the reference signal and machine performance.

The maximum count rate in the measurements was about 150 counts s^{-1} and dead time effects in the detector and preamplifier were negligibly small. The count rate capability of the system was limited by the ADC which was typically busy for about 200 μs per event. Dead time correction in the TAC and ADC was done in a straight forward manner, the correction factor at each position being given by the ratio of the scaler count from the positive logic output of the constant fraction timing discriminator to the integrated count in the time distribution. The dead time correction for the threshold detector was less than 1 per cent and for the broad range detectors, was less than 3 per cent.

For most of the measurements, the preset monitor counts were greater than 10^5 so that the statistical error associated with the monitor was less than 0.3 per cent. The statistical error in the channel counts for a preset monitor count was handled in the usual manner.

The uncertainty in the positioning of the detectors was estimated to be about ± 1 mm. The corresponding errors in the channel counts depend on the spatial position of the measurements and were less than 0.6 per cent.

Fluctuation in the machine voltage, beam current and pulse shape gave rise to uncertainty in the timing of the reference signal. The beam energy was stabilised to an accuracy of ± 5 keV

at 2.8 MeV. With the beam pickoff unit at 0.4 m from the target, the corresponding timing error was only ± 0.02 ns. In all the measurements, the beam current was fairly steady. Although each set of measurements normally extended over three days, the fluctuation in the pulse shape was small. The estimated long term time drift due to all these changes was less than 0.4 ns.

Except for the dead time correction, the other errors listed were random errors. These errors were incorporated into the weights used in the least square Fourier analysis. The resulting error on the amplitude of the fundamental mode ranges from 0.5 per cent at the peak of the time distribution to 4 per cent at 100 ns after the peak for the threshold detector. For the broad range detectors, the error varied from 0.3 per cent at the peak to 1.2 per cent at 200 ns after the peak.

4.2 Nonlinearity of the TAC

The differential nonlinearity of the TAC-ADC system was measured to be within 1 per cent from 10 per cent to 90 per cent of the 1 μs time range. This gave rise to a difference of up to 1 per cent in the width of any channel with respect to that of any other channel. Since the spatial distribution at a given channel was fitted independently of all other channels, the error due to the nonlinearity of the TAC cannot be included in the Fourier analysis. However, it must be considered when describing the time dependence of the various Fourier modes. Rather than apply small errors to the width of each channel it was decided to treat the error as a random error on the channel width and add it to the errors associated with the amplitude of the Fourier modes in the usual manner. The compounded error on the amplitude of the fundamental mode ranges from 1.1 per cent at the peak to 4.1 per cent at 100 ns after the peak for the ^{237}Np detector and from ~ 1 per cent at the peak to ~ 1.5 per cent at 200 ns after the peak for the nonthreshold detectors.

4.3 Systematic Error Associated with Background and Overlap Correction

These measurements were performed at a repetition rate of 1 MHz and, as a consequence, the reaction rate of the broad range detectors following the injection of a particular neutron pulse into the thorium assembly did not decay to a negligible level before the injection of the following neutron pulse. In the case of the ^{235}U detector, for example, the prepulse reaction rate was ~ 0.1 per cent of the peak reaction rate and ~ 4 per cent of the reaction rate at 200 ns after the peak. The prepulse reaction rate is that reaction rate which immediately precedes the increase in reaction rate associated with the injection of a neutron pulse into the assembly. It is also, because of the repetitive pulsing method used in the experiment, the reaction rate at late times after the injection of the neutron pulse.

A correction for the overlap effect described above and for background was made in the following manner to the data obtained at each spatial position with the ^{235}U and ^{239}Pu detectors. The 'late time' decay of the detector reaction rate was fitted with an exponential, extrapolated over the 200 ns time interval of interest and subtracted from the raw experimental data. Since for each measurement, the background was low and the statistical accuracy correspondingly poor the exponent used in all cases was that obtained by summing the 'late time' data from all

thirty-nine spatial positions and fitting a single exponential to the result. No such correction was necessary to the data obtained with the ^{237}Np detector.

Subtraction of a constant background which was extrapolated from 'late times' into the time region of interest was also performed to indicate the magnitude of any systematic error associated with the background correction. The difference in the instantaneous decay constant of the fundamental mode, at times immediately after the peak in the reaction rate, was found to be ~ 0.5 per cent and ~ 3 per cent at 200 ns after the peak. These discrepancies are less than the errors on the instantaneous decay constant of the fundamental mode which are 2 per cent and 5 per cent at the respective times.

4.4 Error Analysis in the Exponential Fitting Routine

In the determination of the instantaneous decay constant $\lambda(t)$ of a reaction rate at a given position, the error analysis incorporated dead time correction, statistical error in the channel counts, timing uncertainty associated with the reference signal and nonlinearity of the TAC. For the fundamental mode the weight applied at each channel was simply the inverse of the square of the error at that channel obtained as explained in Sections 4.1 and 4.2. Near the peak, the error on $\lambda(t)$ for all the reaction rates was ~ ± 2 per cent. At 100 ns after the peak, the error on $\lambda(t)$ was ± 4.4 per cent for ^{237}Np and ±3.0 per cent for the broad range detectors. At 200 ns after the peak the error in $\lambda(t)$ for the broad range detectors was ±5.0 per cent.

4.5 Detector Timing Uncertainty

A source of error which was not included in the error analysis was the detector timing uncertainty (see Section 2.4). This results in a systematic broadening of the time distributions and should be included in any theoretical calculation intended for comparison with the present experimental results.

5. DISCUSSION OF RESULTS

The form of the time dependent amplitudes of the three-dimensional Fourier modes presented in Figure 4 demonstrates that the fission rates were dominated by the contribution associated with the fundamental mode from quite early times after the pulse. In addition, it is apparent that, even though neutron production from the thick target ^{9}Be (d,n) ^{10}B reaction was strongly peaked in the forward direction, the neutron population in the assembly settled into an essentially symmetric spatial distribution quite quickly. In the case of the ^{237}Np fission rate, for instance, the amplitude of the largest of the higher modes was only 3 per cent of that of the fundamental mode at 35 ns after the peak of $R_{111}(t)$. From Figure 5, which shows the instantaneous decay constant for ^{235}U at three positions in the stack, it is again apparent that the contributions for the higher modes were small in comparison to the contribution from the lowest mode for times later than 100 ns after the peak of the fundamental mode since the time distributions at the three positions decayed in much the same way. The initial difference in the decay at $x = +100$ mm was the result of the anisotropic neutron source.

The instantaneous decay constant, $\lambda(t)$, of the fundamental mode for ^{237}Np (Figure 6 a) decreased with time generally, showing that the lowest mode is non-exponential. However, from

almost 40 ns to 65 ns after the peak of the fundamental, $\lambda(t)$ was fairly constant being about $5.1 \times 10^7\ s^{-1}$. Since in this time interval the neutron spectrum in the thorium stack peaks just above 400 keV, the pseudoexponential behaviour may be due to the dominating contribution from this group of neutrons just above the fission threshold of ^{237}Np.

It should be pointed out at this stage that the ^{237}Np fission threshold is not a threshold in the strict sense of the word. The fission cross section decreases sharply below 400 keV, but the cross section is non-negligible in the lower energy region. Thus, as the neutron spectrum in the stack shifts below 400 keV due to inelastic and elastic down scatter, the contribution from neutrons below 400 keV becomes more significant. This may be the cause for the slower decay at later times ($\sim$ 65 ns) and the consequent departure from the pseudoexponential behaviour.

The pseudoexponential behaviour of the ^{237}Np fission rate observed in thorium may be similar to that observed by Gozani (1969) in a large sphere of depleted uranium. In Gozani's case, however, this behaviour lasted for a much longer time ($\sim$ 50 ns).

The instantaneous decay constant of the lowest mode is shown as a function of time in Figure 6b for ^{235}U and in Figure 6c for ^{239}Pu. In the case of the ^{235}U fission rate, $\lambda(t)$ decreased nearly monotonically with time. The $\lambda(t)$ for ^{239}Pu, however, exhibited oscillations at late times ($\sim$ 150 ns after the peak of R_{111}). These oscillations were significantly greater than the error on the decay constant. Similar oscillations were also observed in the exponential fitting of the time distributions at the individual positions.

The oscillations in the decay constant for ^{239}Pu (and less apparently for ^{235}U) are difficult to explain. The counting statistics for ^{239}Pu were better than the counting statistics for ^{237}Np and since no such oscillations were apparent in the instantaneous decay constant of the fundamental mode for ^{237}Np, it is unlikely that the oscillations in ^{239}Pu were caused by the fitting procedure.

6. ACKNOWLEDGEMENTS

We wish to thank the technical staff of Physics Division, A.A.E.C. Research Establishment for their assistance during the experiments. One of us, S. P. Moo, is very grateful to the Colombo Plan (Australia) for a post-graduate scholarship, to the Australian Institute of Nuclear Science and Engineering for its generous grant to the University of Tasmania in support of this work and to Drs. K. B. Fenton and A. G. Fenton of the University of Tasmania for their continued interest and support.

7. REFERENCES

Arai, E., Miessner, H. and Beckurts, K. H. (1966). – Nucl. Sci. Engng. 26, 573.

Beckurts, K.H. (1965). – Proc. I.A.E.A. Symp. Pulsed Neutron Research, Vol. 1, p. 3.

Beghian, L.E., Rasmussen, N.C., Thews, R. and Weber, J. (1963 a). – Nucl. Sci. Engng. 15, 375.

Beghian, L.E., Profio, A.E., Weber, J. and Wilensky, S. (1963 b). – Nucl. Sci. Engng. 17, 82.

Beghian, L.E. and Wilensky, S. (1965). – Proc. I.A.E.A. Symp. Pulsed Neutron Research, Vol. II, p. 511.

Beghian, L.E., Hofmann, F. and Wilensky, S. (1967). – Nucl. Sci. Engng. 27, 80.

Bondarenko, I.I. (1964). – 'Group Constants for Nuclear Reactor Calculations', Consultants Bureau (New York).

Deconninck, G., d'Oultremont, P. and Stievenart, M. (1965). – Proc. I.A.E.A. Symp. Pulsed Neutron Research, Vol. II, p. 493.

Gozani, T. (1969). – Nucl. Sci. Engng. 36, 143.

Inada, T., Kawachi, K. and Hiramoto, T. (1968). – J. Nucl. Sci. and Technol., 5, 22.

Kato, W.Y., Meister, H.H., Main, G.W., Russell, Jr. J.L. and Crosbie, K.L. (1965). – Proc. I.A.E.A. Symp. Pulsed Neutron Research, Vol. II, p. 373.

Miessner, H. and Arai, E. (1966). – Nukleonik 8, 428.

Moo, S.P., Rainbow, M.T. and Ritchie, A.I.M. (1972). – AAEC/TM613.

Napolitano, C.M., Carroll, E.E. and Ohanian, M.J. (1969). – Trans. Am. Nucl. Soc. 12, 256.

Napolitano, C.M., Carroll, E.E. and Ohanian, M.J. (1970). – Trans. Am. Nucl. Soc. 13, 275.

Norton, D.S. (1968). – AAEW–M824.

Rainbow, M.T. and Ritchie, A.I.M. (1971). – J. Nucl. Energy 25, 461.

Ritchie, A.I.M. and Moo, S.P. (1972). – To be submitted to J. Nucl. Energy.

Rush, C.J. (1964). – Rev. Scient. Instrum., 35, 149.

TABLE 2.

TIME DEPENDENT AMPLITUDES OF THE THREE-DIMENSIONAL FOURIER MODES FOR NEPTUNIUM-237, URANIUM-235 AND PLUTONIUM-239

CHANNEL NUMBER	NEPTUNIUM-237 (2.49 NS/CH)		URANIUM-235 (2.49 NS/CH)		PLUTONIUM-239 (2.36 NS/CH)	
	R111	ERROR	R111	ERROR	R111	ERROR
7	4755.6	54.1	25680.1	267.9	2638.1	87.8
8	5447.2	59.3	28391.3	291.5	5992.9	159.0
9	5923.2	63.3	29688.4	302.2	8735.6	123.9
10	6075.9	65.5	30150.9	306.5	9603.5	102.0
11	5917.7	66.2	29509.9	300.4	9350.1	100.0
12	5443.1	63.0	28458.1	290.0	8742.0	94.4
13	4778.0	57.4	26976.4	275.4	8127.2	87.2
14	4065.5	49.6	25488.8	260.2	7494.0	80.4
15	3401.2	42.4	23793.3	243.3	6953.3	74.3
16	2804.1	35.3	22220.3	227.0	6491.8	69.0
17	2300.9	29.0	20853.0	213.1	5992.9	64.0
18	1927.3	24.9	19540.6	199.7	5561.9	59.5
19	1594.2	20.8	18308.4	187.1	5207.1	55.6
20	1342.9	17.7	17181.6	175.7	4870.6	52.2
21	1154.9	15.6	16124.3	165.0	4591.4	49.2
22	994.1	14.0	15164.6	155.3	4320.6	46.5
23	839.4	11.9	14337.8	146.9	4056.6	43.8
24	736.8	10.8	13514.9	138.6	3853.8	41.6
25	648.1	9.9	12812.9	131.4	3627.1	39.4
26	565.9	8.9	12181.0	125.0	3456.1	37.5
27	497.0	8.1	11522.3	118.5	3299.3	35.9
28	439.8	7.4	10990.9	113.0	3104.6	34.1
29	387.0	6.8	10496.1	108.0	2951.1	32.4
30	334.9	6.1	10029.0	103.4	2771.0	30.7
31	301.2	5.8	9522.6	98.3	2643.1	29.3
32	259.4	5.1	9130.8	94.3	2530.1	28.1
33	231.8	4.9	8666.5	89.7	2401.1	26.8
34	197.9	4.3	8316.8	86.1	2314.0	25.9
35	184.1	4.2	7941.5	82.4	2183.1	24.7
36	164.9	3.9	7582.2	78.8	2087.2	23.7
37	140.2	3.5	7309.2	76.0	1969.9	22.5
38	125.6	3.3	7005.3	72.9	1888.0	21.6
39	110.9	3.1	6688.8	69.8	1805.1	20.8
40	103.7	3.0	6430.5	67.2	1749.9	20.2
41	89.2	2.7	6161.2	64.5	1671.2	19.4
42	78.9	2.6	5918.7	62.0	1559.8	18.4
43	76.1	2.5	5753.4	60.3	1511.2	17.7
44	68.1	2.3	5492.9	57.8	1457.4	17.2
45	61.0	2.2	5329.2	56.1	1370.5	16.4
46	56.6	2.1	5144.5	54.2	1331.0	15.9
47	51.5	2.0	4961.6	52.4	1262.1	15.2
48	46.4	1.9	4785.2	50.6	1215.0	14.7
49	42.3	1.9	4615.3	48.9	1156.4	14.1
50	39.3	1.7	4462.1	47.4	1114.3	13.7
51	36.6	1.7	4298.2	45.8	1078.6	13.3
52	33.1	1.6	4145.6	44.2	1041.0	12.9
53	30.4	1.5	4053.6	43.3	997.0	12.5
54	27.3	1.4	3867.7	41.5	971.5	12.2
55	28.8	1.5	3777.7	40.5	934.8	11.8

TABLE 2.(CONT.)

TIME DEPENDENT AMPLITUDES OF THE THREE-DIMENSIONAL FOURIER MODES FOR NEPTUNIUM-237, URANIUM-235 AND PLUTONIUM-239

CHANNEL	NEPTUNIUM-237 (2.49 NS/CH)		URANIUM-235 (2.49 NS/CH)		PLUTONIUM-239 (2.36 NS/CH)	
NUMBER	R111	ERROR	R111	ERROR	R111	ERROR
56	22.5	1.3	3628.1	39.0	898.1	11.5
57	23.1	1.3	3525.4	38.0	870.2	11.2
58	21.1	1.2	3414.6	36.9	859.7	11.1
59	19.8	1.2	3305.8	35.8	820.7	10.7
60	16.5	1.1	3252.1	35.2	784.0	10.3
61	18.3	1.1	3125.3	34.0	763.6	10.1
62			3038.3	33.1	733.9	9.8
63			2957.5	32.3	714.3	9.6
64			2878.9	31.5	701.5	9.4
65			2774.7	30.4	668.9	9.1
66			2693.2	29.6	666.9	9.0
67			2617.9	28.8	635.4	8.8
68			2525.0	27.9	615.0	8.5
69			2476.0	27.4	599.8	8.3
70			2390.0	26.6	584.8	8.2
71			2332.8	26.0	566.1	8.0
72			2288.2	25.5	538.3	7.7
73			2218.1	24.8	506.6	7.4
74			2169.4	24.3	506.0	7.3
75			2106.8	23.7	491.2	7.2
76			2048.7	23.1	473.0	7.0
77			2028.3	22.9	448.6	6.8
78			1957.2	22.2	450.6	6.7
79			1882.2	21.4	431.2	6.5
80			1942.2	22.1	422.8	6.5
81			1764.5	20.4	414.0	6.4
82			1826.0	20.9	399.3	6.2
83			1730.6	19.9	390.9	6.1
84			1644.6	19.0	375.3	5.9
85			1675.2	19.3	378.2	6.0
86			1589.7	18.5	367.6	5.8
87			1533.8	17.9	360.6	5.8
88			1535.3	17.9	345.1	5.6
89			1448.2	17.1	330.9	5.4
90			1442.8	17.0	328.5	5.4
91			1431.7	16.9	320.8	5.3
92			1388.8	16.4	310.5	5.2
93			1384.4	16.4	293.5	5.0
94			1307.5	15.6	293.7	5.0
95			1316.5	15.7	276.9	4.8
96			1267.6	15.2	277.5	4.8
97			1246.7	15.0	274.8	4.8
98			1204.6	14.6	259.9	4.6
99			1161.1	14.1	259.0	4.6
100			1162.7	14.1	253.1	4.5
101			1112.5	13.6	250.2	4.5
102			1122.9	13.7	240.8	4.4
103			1081.2	13.3	234.0	4.3
104			1074.1	13.2	237.4	4.4

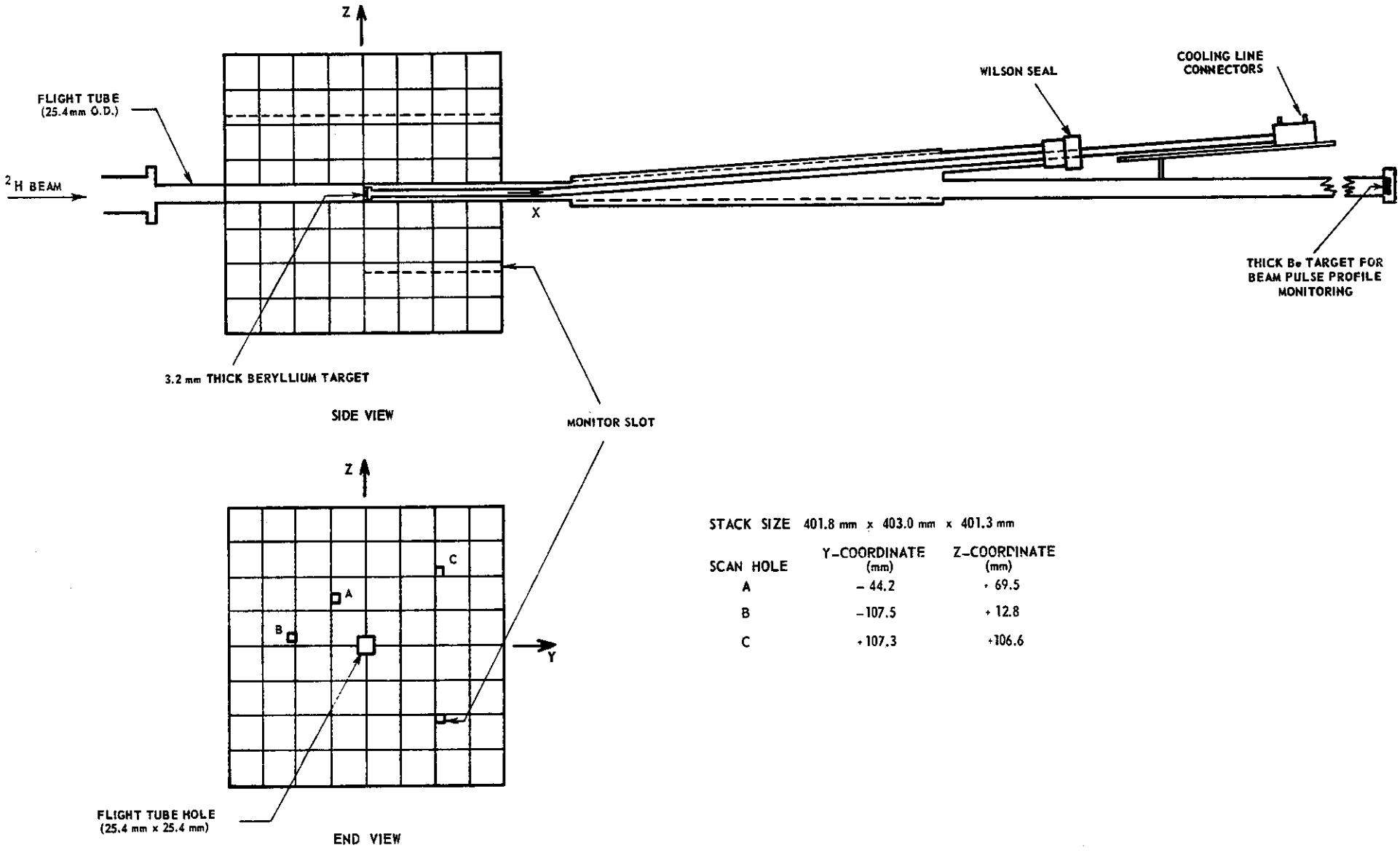

STACK SIZE 401.8 mm x 403.0 mm x 401.3 mm

SCAN HOLE	Y-COORDINATE (mm)	Z-COORDINATE (mm)
A	− 44.2	+ 69.5
B	−107.5	+ 12.8
C	+ 107.3	+106.6

FIGURE 1 SCHEMATIC DIAGRAM OF THE THORIUM ASSEMBLY

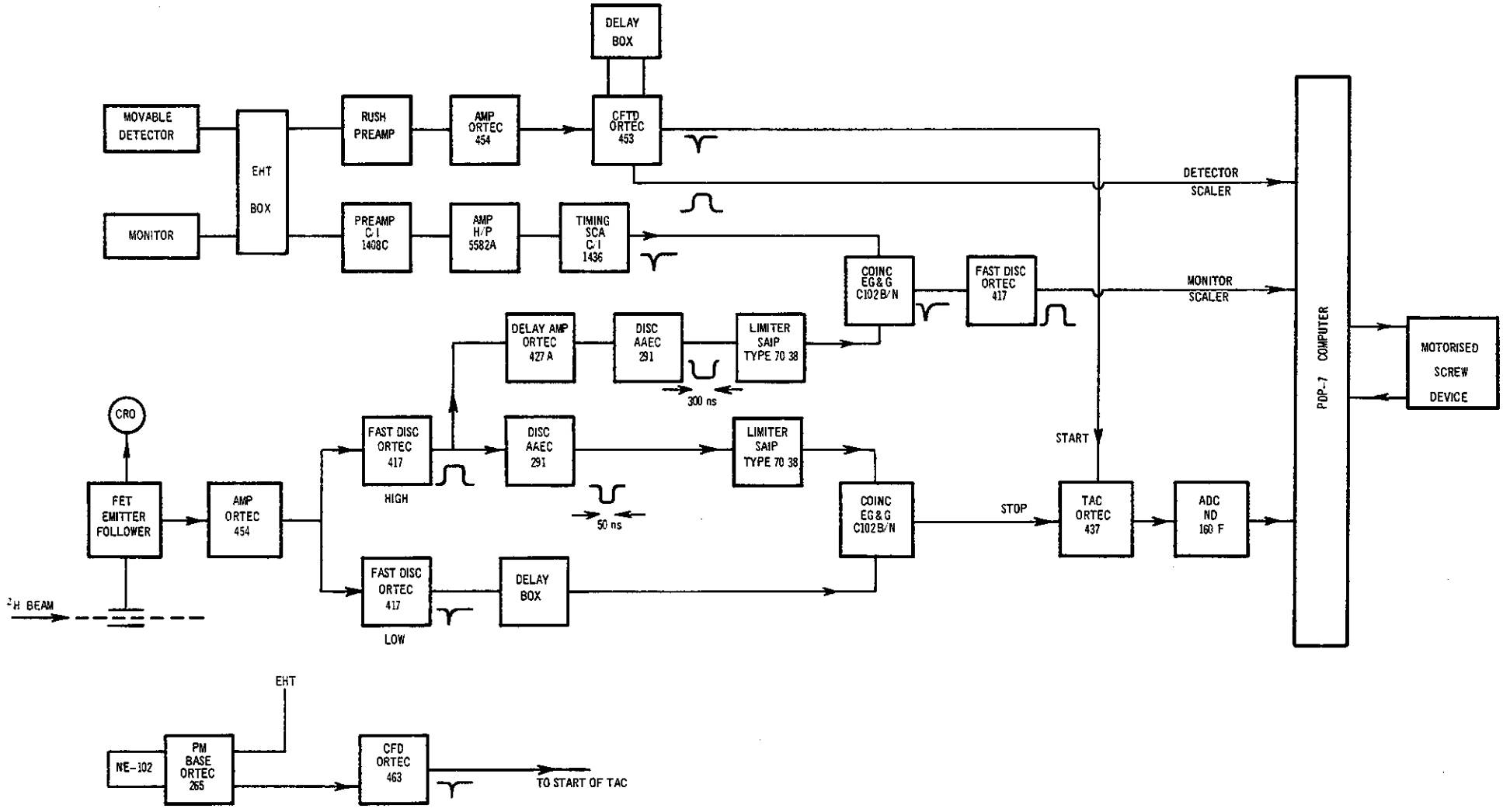

FIGURE 2 BLOCK DIAGRAM OF THE ELECTRONIC SYSTEM

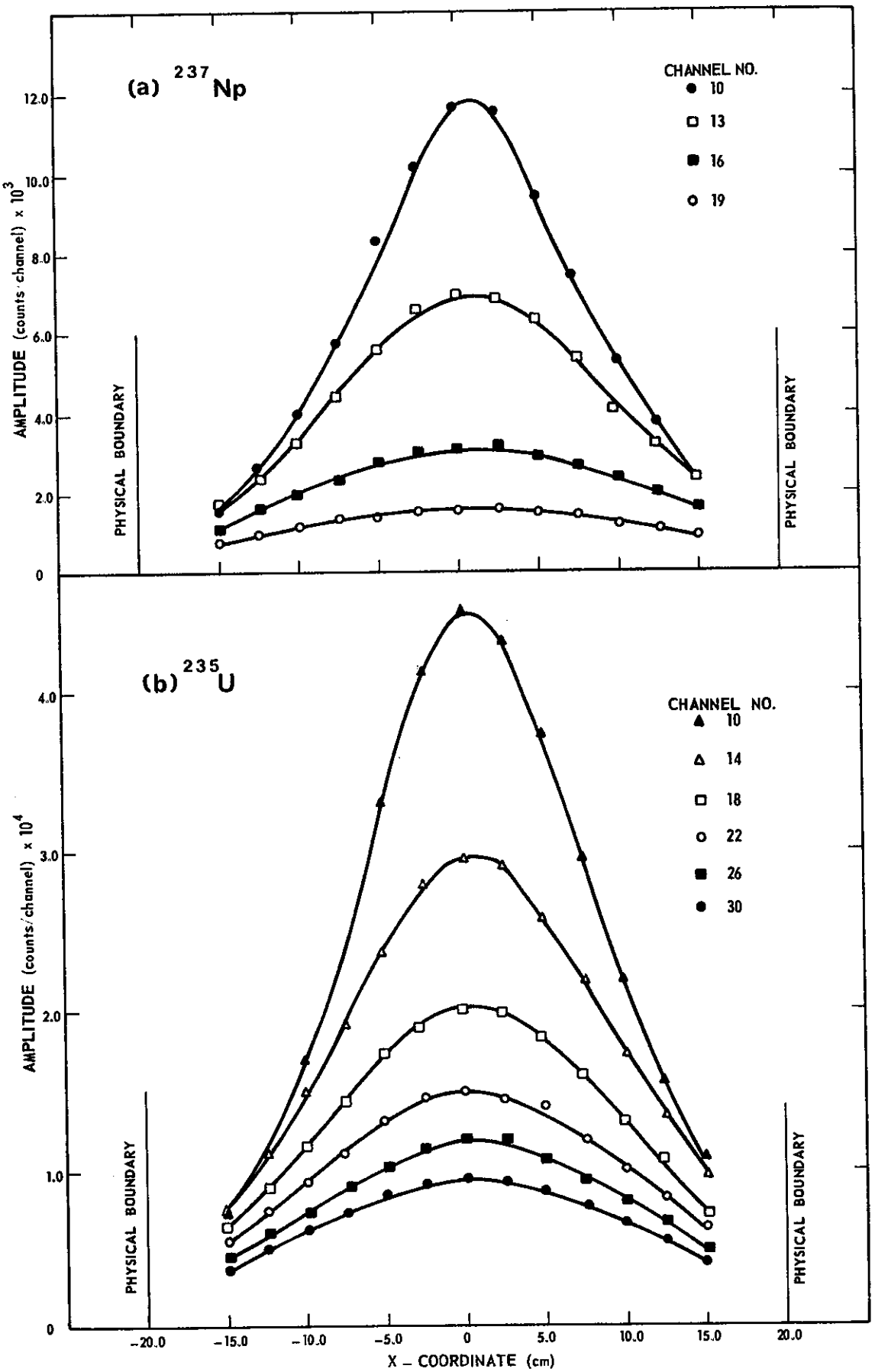

FIGURE 3. SPATIAL DISTRIBUTIONS OF (a) ^{237}Np AND (b) ^{235}U FISSION RATES MEASURED ALONG SCAN HOLE A AT VARIOUS TIMES WITH RESPECT TO THE PULSE

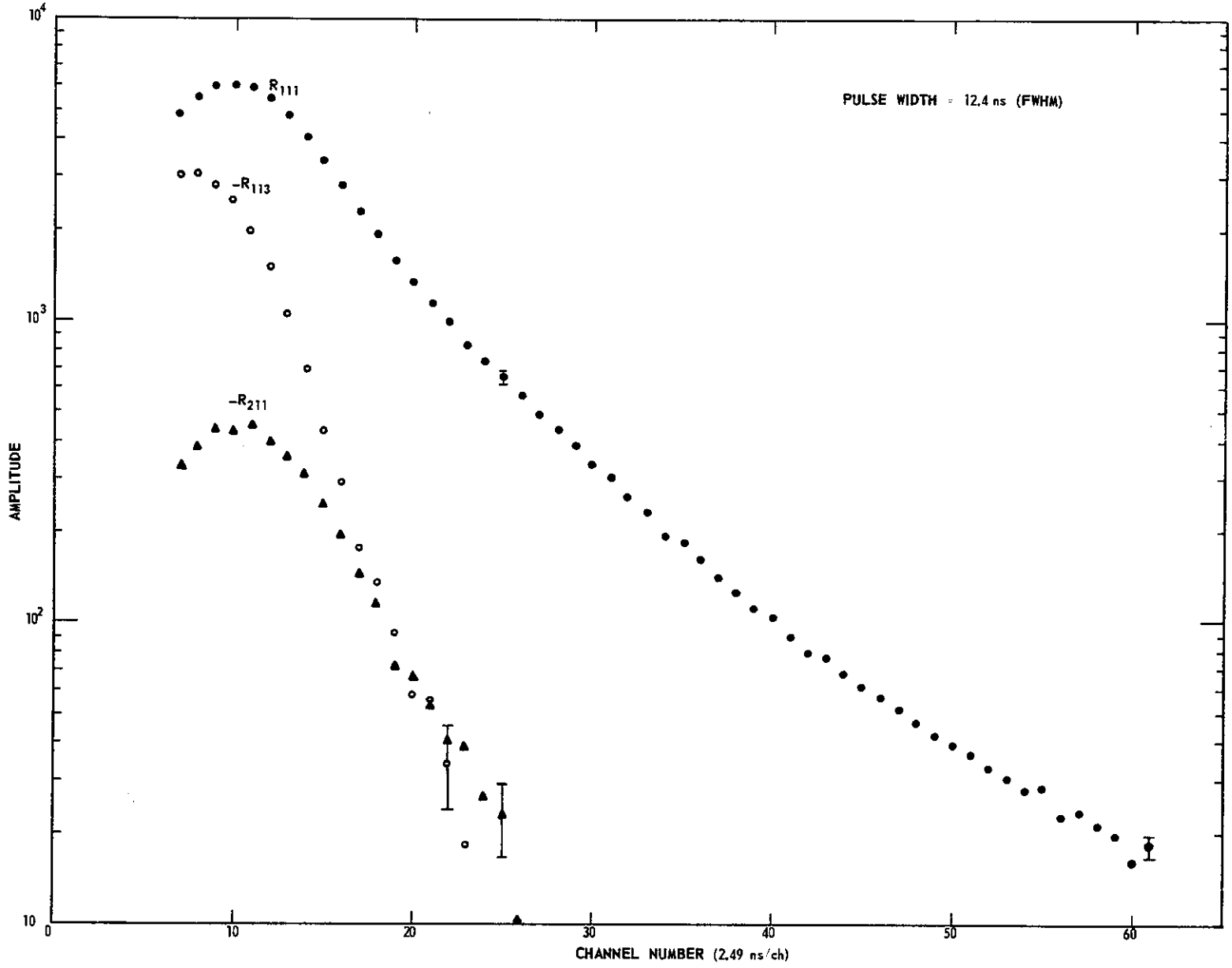

FIGURE 4a TIME DEPENDENT AMPLITUDES OF THE THREE-DIMENSIONAL FOURIER MODES FOR ^{237}Np

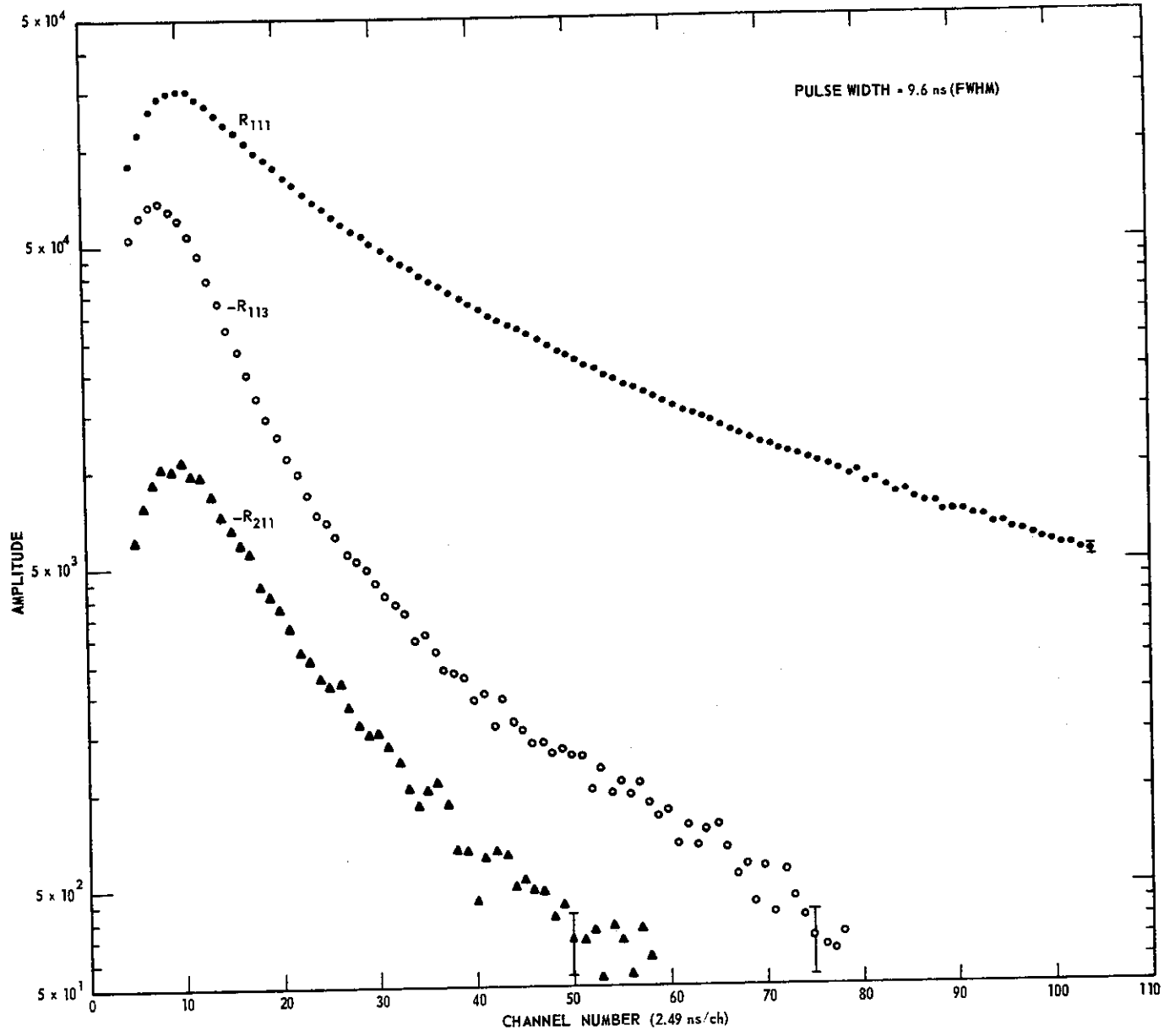

FIGURE 4b TIME DEPENDENT AMPLITUDES OF THE THREE-DIMENSIONAL FOURIER MODES FOR ^{235}U

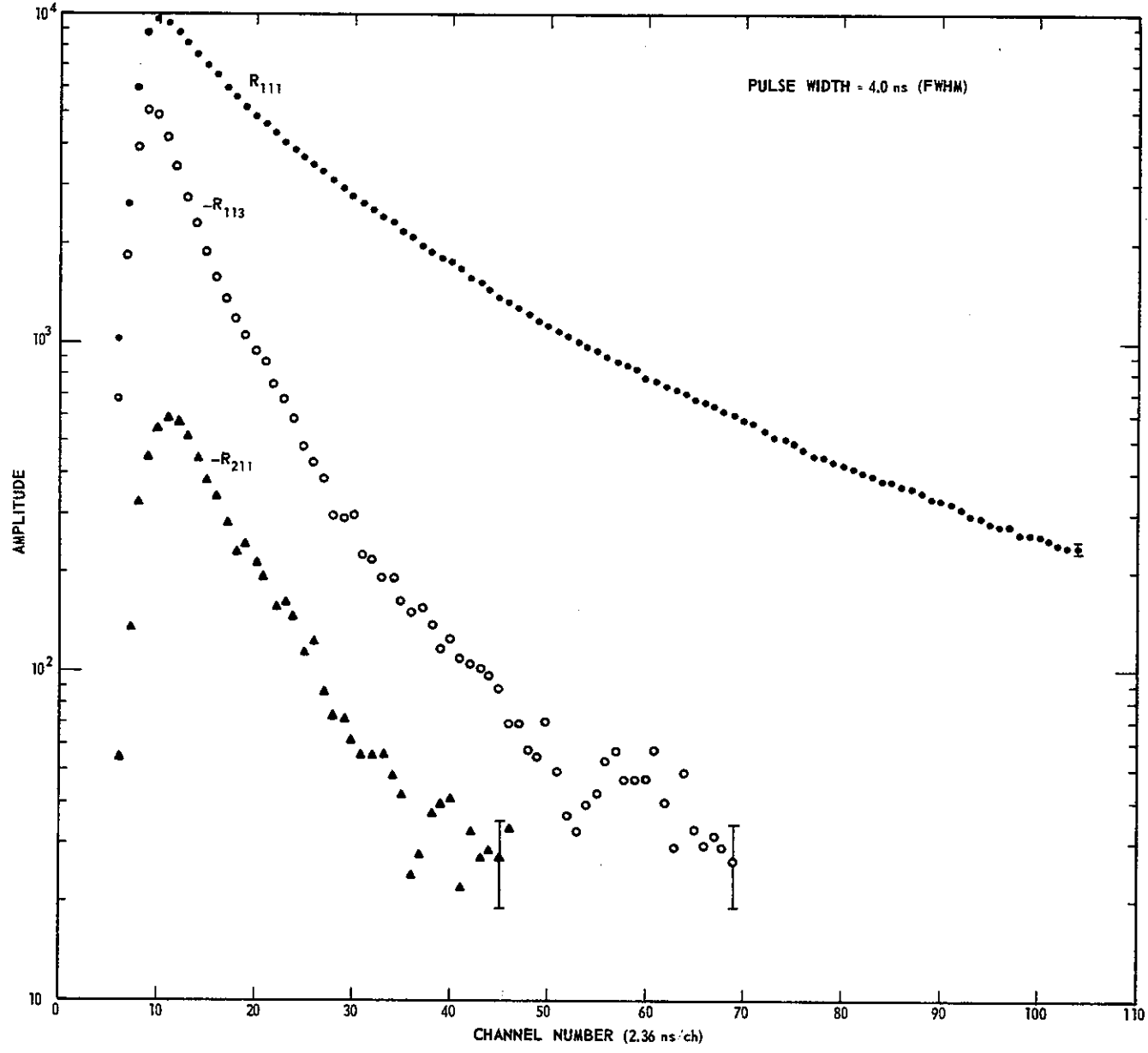

FIGURE 4c TIME DEPENDENT AMPLITUDES OF THE THREE-DIMENSIONAL FOURIER MODES FOR ^{239}Pu

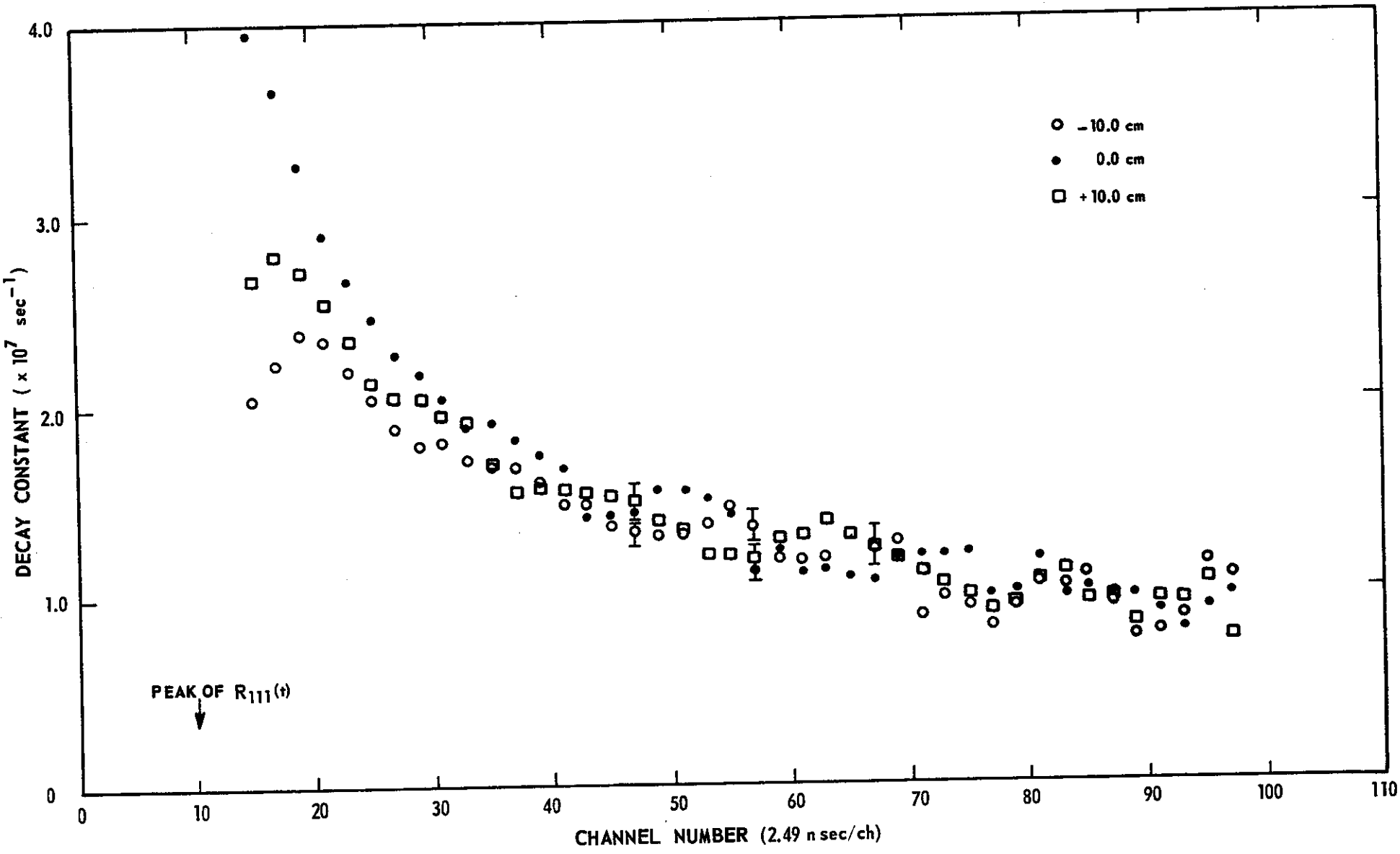

FIGURE 5 TIME DEPENDENT INSTANTANEOUS DECAY CONSTANTS OF THE ^{235}U FISSION RATE AT THREE POSITIONS ALONG SCAN HOLE A

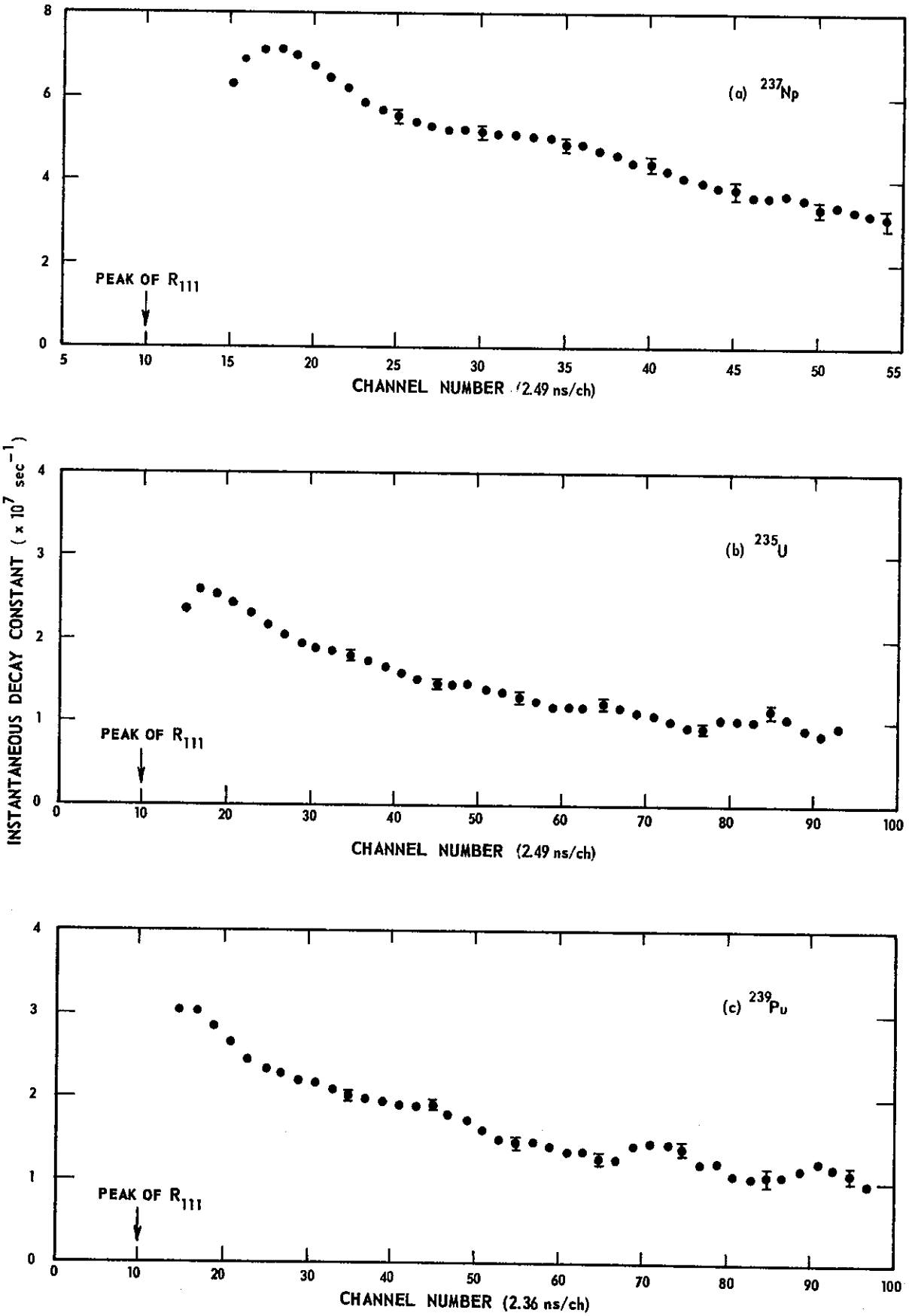

FIGURE 6 TIME DEPENDENT INSTANTANEOUS DECAY CONSTANTS OF THE FUNDAMENTAL MODE FOR (a) ^{237}Np, (b) ^{235}U AND (c) ^{239}Pu